Lithium-ion Battery Instantaneous Available Power Prediction Using Surface Lithium Concentration of Solid Particles in a Simplified Electrochemical Model

Linfeng Zheng, *Student Member, IEEE*, Jianguo Zhu, *Senior Member, IEEE*, Guoxiu Wang, Dylan Dah-Chuan Lu, *Senior Member, IEEE*, and Tingting He, *Student Member, IEEE*

***Abstract*—Accurate battery power capability prediction can contribute to reliable and sufficient utilization of the battery to absorb or deliver a certain amount of power within its safe operating area. The power capability of a battery is a finite quantity that is limited by the electrochemical reaction properties occurring inside the battery. Note that the instantaneous available power of the battery is strongly related to the surface lithium concentration of solid particles in battery electrodes, but their relationship has not been explored sufficiently yet. This paper proposes a novel method for battery instantaneous available power prediction using a practical physical limit (i.e., lithium concentration limit) rather than the limits of macroscopically observed variables, such as the cell terminal voltage and current, thus providing a direct insight into electrochemical processes inside batteries. The surface lithium concentration of the solid particle is derived from a simplified battery electrochemical model, and a relationship between battery instantaneous available power and surface lithium concentration is quantified for the power capability prediction. Promising results with small forecast errors can be achieved for battery charging and discharging at different cell aging levels and ambient temperatures, which highlights the superior accuracy and robustness of the proposed method.**

***Index Terms*—Battery management system (BMS), instantaneous available power prediction, lithium concentration limit, lithium-ion battery, surface lithium concentration.**

I. Introduction

LITHIUM-ION batteries with desirable performance in energy density, power density, and cycle life are ubiquitous in electrical energy storage applications, such as smart grids, electric vehicles, and railway transportation systems [1]–[3], etc. Precisely because large amounts of power and energy are required in these applications, lithium-ion battery management systems (BMSs) with essential functions including cell balancing, state of charge (SOC) estimation, state of health estimation, and state of available power prediction, etc., are necessary to ensure safe and efficient battery operations [4]–[10]. State of available power reports the peak power capability of the battery that can be delivered to loads or absorbed from regenerative braking or active recharging within a time horizon of interest [11]. Thus, it is of great significance to accurately predict battery available power for reliable and optimal utilization of the battery.

The reported techniques for predicting battery available power can generally be classified into three groups including characteristic map-based methods, machine learning methods, and model-based methods. The characteristic map-based methods utilize static interdependencies between battery available power and its influenced factors, such as SOC, temperature, and cell aging to build a multidimensional power capability map [9], which can be directly stored in the memory of BMSs. Due to their simplicity and ease of implementation, the characteristic map-based methods are prevailingly adopted by manufacturers of battery and BMS. However, the characteristic map-based methods have limited adaptive capability against dynamic conditions and require a high amount of nonvolatile memory to store the multidimensional map [12]. The machine learning methods including neural network and support vector machine have been developed for battery available power prediction in [13]–[16]. Approximate relationships between battery available power and input variables, such as cell terminal voltage, internal resistance, and SOC, temperature, etc., can be quantitatively trained with reliable experimental data, but the accuracy of the prediction depends firmly on the training data. Alternatively, a battery model is employed in the model-based methods to predict dynamic behaviors of the battery for computing its peak power capability within the design limits such as the permitted highest and lowest values of cell terminal voltage, current, and SOC, etc. [17]–[20]. The model-based methods have attracted considerable attentions due to their high adaptation capabilities and real-time performance. The main differences among the model-based methods are the type of battery model and the estimation technique of battery states and model parameters. Farmann *et al.* [9] summarized and compared different adaptive joint and dual-estimation techniques including Kalman

Manuscript received September 7, 2017; revised December 4, 2017; accepted January 2, 2018. Date of publication January 11, 2018; date of current version August 7, 2018. This work was supported by the Rail Manufacturing Cooperative Research Centre. Recommended for publication by Associate Editor F. H. Khan. *(Corresponding author: Linfeng Zheng.)*

L. Zheng is with the Faculty of Engineering and Information Technology and the Centre for Clean Energy Technology, University of Technology Sydney, Sydney, NSW 2007, Australia (e-mail: Linfeng.Zheng@student.uts.edu.au).

J. Zhu, D. D.-C. Lu, and T. He are with the Faculty of Engineering and Information Technology, University of Technology Sydney, Sydney, NSW 2007, Australia (e-mail: Jianguo.Zhu@uts.edu.au; Dylan.Lu@uts.edu.au; Tingting.He@student.uts.edu.au).

G. Wang is with the Centre for Clean Energy Technology, University of Technology Sydney, Sydney, NSW 2007, Australia (e-mail: Guoxiu.Wang@uts.edu.au).

Color versions of one or more of the figures in this paper are available online at http://ieeexplore.ieee.org.

Digital Object Identifier 10.1109/TPEL.2018.2791965

filter-based approaches, least-square-based approaches, and other filters and observers for the model-based power prediction methods. It is noteworthy that equivalent circuit models (ECMs) are typically employed in these model-based methods since they have simple and flexible structures as well as few unknown variables [21]. However, ECMs idealize battery by applying circuit elements to represent its electrical behaviors but offer little physical explanation of battery performance, thus leading to limited prediction capability [22], [23].

Moreover, the power capability of a battery is a finite quantity that is limited by the chemical reaction properties occurring inside the battery [16]. However, the reported techniques of battery power prediction are primarily derived based on the limits of macroscopically observed variables, such as cell terminal voltage and current, which are insufficient to adequately depict the electrochemical processes inside batteries, and consequently, the resulting battery power forecasts may be conservative. To enhance the safety, efficiency, and longevity of the battery system, an advanced BMS with physical insight into batteries should be developed, and a practical physical limit of the battery is highly required for reliable battery power capability prediction. In lithium-ion batteries, high power requires that the lithium diffusion in and out of solid particles of battery electrodes takes place fast enough to supply the loading current [24]. Lithium concentrations within the inner regions of solid particles differ substantially from surface concentration during high current rate, and solid phase concentration gradients requires time to relax [23]. Based on the assumption that lithium ions within the inner regions of solid particles fail to fleetly diffuse to the surface of the solid particles for instantaneous applications, the surface lithium concentration can be employed for describing battery instantaneous power capability. It has also been reported that battery instantaneous available power depends significantly on the surface lithium concentration [25]. However, the relationship between the surface lithium concentration and battery instantaneous available power has not been explored sufficiently yet.

It is also worth mentioning that the aforementioned methods have rarely discussed the effects of power dissipation on battery internal resistance in battery available power prediction. Although many equivalent circuit model-based methods have considered the internal resistance and polarization resistance for peak power prediction, the resistances used in the equivalent circuit model-based methods are mainly employed for determining the maximum/minimum current within the permitted limited voltages rather than directly computing the power dissipation on the resistances. Since the internal resistance is a primary source of power dissipation [26], there is no doubt that battery available power prediction would be problematic due to the omission of power dissipation on battery internal resistance, especially in the prediction of battery instantaneous available power with large loading current.

The primary goal of this paper is to address the previously mentioned issues and investigate a battery power prediction method from a perspective of physical mechanism-based reactions inside the battery using a physical limit, namely lithium concentration limit. Based on the theoretical analysis of battery Gibbs power and dissipation power of its internal resistance, the relationship between the surface concentration and instantaneous available power is quantified for battery charge and discharge power capabilities prediction. The proposed method is then experimentally verified with various cell aging levels and ambient temperatures.

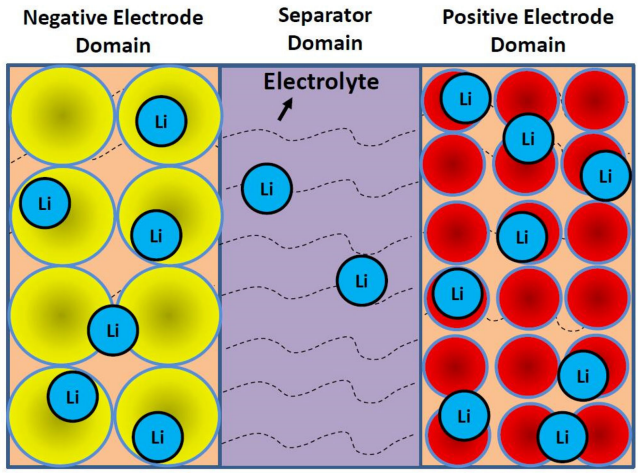

Fig. 1. Schematic of a lithium-ion battery EM.

The rest of the paper is organized as follows: Section II introduces a simplified battery electrochemical model (EM) for computing lithium concentrations of various nodes of battery spherical solid particles, which was mainly developed in our previous work [22]. The analysis and modeling processes of the proposed battery instantaneous available power prediction are outlined in Section III. Section IV discusses the experimental verification of the proposed method, followed by the conclusions drawn in Section V.

II. Battery EM and Lithium Concentration

A. Battery EM

A lithium-ion battery EM consisting of a negative electrode with solid $\mathrm{Li}x\mathrm{C}_6$ particles, an electron-blocking separator, and a positive electrode with solid metal oxide particles is depicted in Fig. 1. During a battery discharge process, lithium ions deinsert from the solid $\mathrm{Li}x\mathrm{C}_6$ particles in the negative electrode, travel via diffusion, and migration through the electrolyte across the separator to the positive electrode where they insert into the solid metal oxide particles. Simultaneously, electrons, blocked by the separator, transfer from the negative electrode to the positive electrode through an external circuit. During a battery charge process, the opposite moving processes of lithium ions and electrons occur.

Coupled nonlinear partial differential equations are inevitably used in the lithium-ion battery EM for describing underlying dynamics of the battery, thus leading to the expensive computation and impracticability of the model [27]. To reduce the computational complexity, a simplified lithium-ion battery EM, known as single particle model (SPM), has been widely investigated in the literature [22], [23], [25]–[27]. In the SPM, each electrode is idealized as a single spherical solid particle, which can

TABLE I
GOVERNING EQUATIONS FOR COMPUTING THE LITHIUM CONCENTRATION OF THE SOLID PARTICLE [22]

Equation		Description
$dr = R_p/\text{node}$	(1)	Node meshing of radius
$\frac{\partial c_s(r,t)}{\partial t} = D_s\left(\frac{2}{r}\frac{\partial c_s(r,t)}{\partial r} + \frac{\partial^2 c_s(r,t)}{\partial r^2}\right)$	(2)	Solid phase transport of lithium
$\frac{\partial c_s(r,t)}{\partial t} = \frac{c_{sd}(i,k+1)-c_{sd}(i,k)}{dt}$	(3)	Lithium changing with time
$\frac{\partial c_s(r,t)}{\partial r} = \frac{c_{sd}(i+1,k)-c_{sd}(i-1,k)}{2dr}$	(4)	Lithium changing with space
$\frac{\partial^2 c_s(r,t)}{\partial r^2} = \frac{c_{sd}(i+1,k)-2c_{sd}(i,k)+c_{sd}(i-1,k)}{dr^2}$	(5)	Lithium changing with space
$c_{s\_\text{mean}} = \sum_{i=1}^{\text{node}} 3c_{sd}(i,k)(i-1)^2 dr^3/R_p^3$	(6)	Mean concentration
$\begin{cases} \frac{c_{sd}(2,k)-c_{sd}(1,k)}{dr} = 0 \\ \frac{c_{sd}(\text{node},k)-c_{sd}(\text{node}-1,k)}{dr} = \frac{I((k-1)dt)}{D_s FaL} \end{cases}$	(7)	Boundary conditions
$c_{sd}(i,1) = c_{sd}^0$	(8)	Initial condition

well strike a balance between the mathematical simplicity and modeling accuracy while sufficiently enhancing the state observability [22], [28]. The mean lithium concentration of the solid particle of the SPM has been sophisticatedly applied for battery SOC estimation, and remarkable results with high accuracy can be achieved [22], [28]–[30]. It has been reported that surface lithium concentration of the solid particle is strongly related to the instantaneous power capability of the battery [25], but their relationship has not been investigated sufficiently yet. Thus, this paper focuses on developing the surface lithium concentration of the solid particle for modeling and predicting battery instantaneous available power.

B. Surface Lithium Concentration

As reported in our previous work [22], the lithium concentration at various radii of the solid particle can be obtained by using the discretized governing equations, and the experimental results confidently validated the robustness and availability of the developed SPM, which provides a solid foundation and convincing calculation results of surface concentration for this paper. The governing equations for computing the lithium concentration of the solid particle are briefly listed in Table I, and more details are provided in [22].

In the developed SPM [22], each solid particle was meshed as 40 nodes for equilibrating the model accuracy and computational efforts. Fig. 2 shows the lithium ion concentrations in different nodes of the negative solid particle during battery charge process with the current rate of 1/3 C. As can be observed, the lithium concentration in the outmost node can be acquired during the whole process of battery operation, which is regarded as the surface concentration of the solid particle and is employed to develop the prediction method for battery instantaneous available power capability.

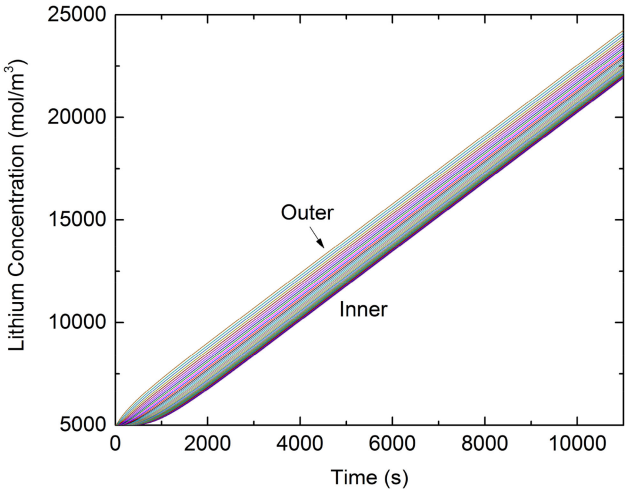

Fig. 2. Lithium ion concentrations in different nodes of the negative solid particle during battery charge process with the current rate of 1/3 C.

III. PROPOSED INSTANTANEOUS AVAILABLE POWER PREDICTION METHOD

The reaction Gibbs free energy of the battery is determined by

$$\Delta G = -nFV_{\text{OCV}} + RT\ln Q_r \tag{9}$$

where ΔG denotes the Gibbs free energy, n the number of electrons transferred, F the Faraday constant, V_{OCV} the open circuit voltage (OCV), R the gas constant, T the absolute temperature, and Q_r the reaction quotient.

If all the Gibbs free energy is converted to work that would be the maximum electrical work, W_{Gibbs}, one has

$$W_{\text{Gibbs}} = -\Delta G = nFV_{\text{OCV}} - RT\ln Q_r. \tag{10}$$

As previously mentioned, the internal resistance of a battery is a primary source of power dissipation, which could not be omitted when applying a large loading current. With this in consideration, the charge and discharge power capabilities of the battery are governed, respectively, by

$$P_{\text{chg}} = P_{\text{Gibbs}} + P_{\text{res}} = \frac{dW_{\text{Gibbs}}}{dt} + P_{\text{res}} \tag{11}$$

$$P_{\text{dis}} = P_{\text{Gibbs}} - P_{\text{res}} = \frac{dW_{\text{Gibbs}}}{dt} - P_{\text{res}} \tag{12}$$

where P_{chg} and P_{dis} denote the charge and discharge power capabilities of the battery, respectively, P_{Gibbs} is the Gibbs power, and P_{res} the power dissipation in battery internal resistance. It is noted that the charge power provides the Gibbs power of the battery reaction and the power dissipation during battery charge process, and the Gibbs power of the battery reaction supports the discharge power and the power dissipation during battery discharge process. The ratios of the Gibbs power to the charge power and the discharge power to the Gibbs power can also be used to evaluate the efficiencies of battery charge and discharge, respectively.

The time horizon is defined as 1 s for the instantaneous power prediction in the presented study. During this instantaneous time horizon, the reaction quotient, Q_r, that is

determined by the concentrations of chemical species involved in the battery reaction is deemed to be not significantly changed and remain constant. Thus, the instantaneous Gibbs power can be arranged as

$$P_{\mathrm{Gibbs}} = \frac{d\left(nFV_{\mathrm{OCV}}\right)}{dt} = FV_{\mathrm{OCV}}\frac{dn}{dt} + nF\frac{dV_{\mathrm{OCV}}}{dt}. \quad (13)$$

With the lithium concentration limit, it is regarded that battery instantaneous available power achieves its peak value when the surface concentration of the solid particle increases to its permitted maximum value. The change of the number of electrons transferred in the instantaneous time horizon is represented by the growing number of lithium ions inserted to the surface of the solid particle, namely

$$\frac{dn}{dt} = \sigma\left(c_{\mathrm{surf,max}} - c_{\mathrm{surf},0}\right) = \sigma\Delta c_{\mathrm{surf}} \quad (14)$$

where $c_{\mathrm{surf},0}$ and $c_{\mathrm{surf,max}}$ denote the initial value and the maximum value of the surface concentration of the solid particle, respectively, Δc_{surf} is the maximum change of the surface concentration which is the difference between $c_{\mathrm{surf,max}}$ and $c_{\mathrm{surf},0}$, and σ is the transformational coefficient between the surface concentration and the number of electrons.

The number of electrons transferred is represented by the mean lithium concentration of the solid particle and can be described as

$$n = \gamma c_{s\_\mathrm{mean}} \quad (15)$$

where γ denotes the transformational coefficient between the number of electrons transferred and the mean lithium concentration of the solid particle, and c_{s_mean} denotes the mean lithium concentration of the solid particle, which can be computed based on the concentration of each node [22], as given by

$$c_{s\_\mathrm{mean}} = \sum_{i=1}^{\mathrm{node}} 3c_{sd}\left(i,k\right)\left(i\ -\ 1\right)^2 dr^3 \big/ R_p^3. \quad (16)$$

The battery OCV change with time can be expressed as

$$\frac{dV_{\mathrm{OCV}}}{dt} = \frac{d\mathrm{SOC}}{dt}\frac{dV_{\mathrm{OCV}}}{d\mathrm{SOC}} = k\Delta c_{\mathrm{surf}}\frac{dV_{\mathrm{OCV}}}{d\mathrm{SOC}} \quad (17)$$

where the SOC change is determined by the maximum change of the surface concentration in the instantaneous time horizon, and k denotes their transformational coefficient. It is noted that in the battery EM, the SOC is represented by the lithium-ion concentrations in electrodes [22]. With the computation results of lithium-ion concentrations, the SOC can be obtained, and then the $dV_{\mathrm{OCV}}/d\mathrm{SOC}$ value in (17) can be determined according to the OCV evolution against SOC values of the battery shown in Fig. 3.

The loading current applied to battery internal resistance is also considered as being determined by the maximum change of the surface concentration in the instantaneous time horizon and, therefore, the power dissipation is given by

$$P_{\mathrm{res}} = i^2 R_{\mathrm{bat}} = \varepsilon{\Delta c_{\mathrm{surf}}}^2 R_{\mathrm{bat}} \quad (18)$$

where i denotes the loading current of the battery, ε the transformational coefficient between the loading current and the maximum change of surface concentration, and R_{bat} denotes the battery internal resistance that refers to battery direct current resistance, which is the sum of the ohmic resistance and the polarization resistance [31]. Different battery internal resistance values may be used for charge and discharge, and are denoted as R_{chg} and R_{dis}, respectively.

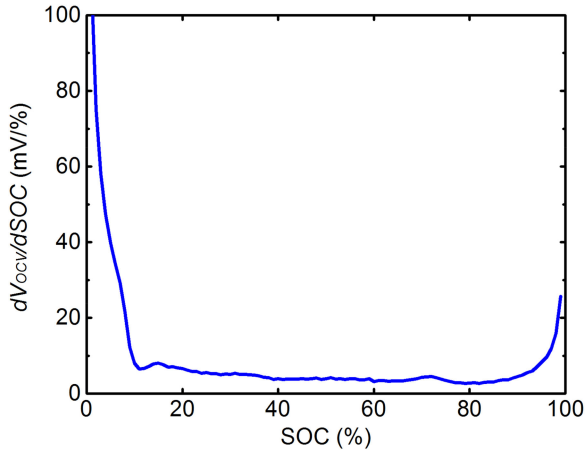

Fig. 3. OCV evolution against SOC values.

As mentioned in the previous section, the lithium ions deintercalate from the negative electrode and intercalate into the positive electrode during battery discharge, and the opposite process occurs during battery charge. Thus, the surface concentration of the positive solid particle is applied for predicting battery discharge power capability, and the surface concentration of the negative solid particle is employed for forecasting battery charge power capability. Combining (11)–(18), the maximum values of instantaneous charge and discharge power capabilities can be expressed as

$$P_{\mathrm{chg,inst}} = \sigma^-\Delta c^-_{\mathrm{surf}}FV_{\mathrm{OCV}} + \lambda^-\Delta c^-_{\mathrm{surf}}c^-_{s\_\mathrm{mean}}F\frac{dV_{\mathrm{OCV}}}{d\mathrm{SOC}} + \varepsilon^-{\Delta c^-_{\mathrm{surf}}}^2 R_{\mathrm{chg}} \quad (19)$$

$$P_{\mathrm{dis,inst}} = \sigma^+\Delta c^+_{\mathrm{surf}}FV_{\mathrm{OCV}} + \lambda^+\Delta c^+_{\mathrm{surf}}c^+_{s\_\mathrm{mean}}F\frac{dV_{\mathrm{OCV}}}{d\mathrm{SOC}} - \varepsilon^+{\Delta c^+_{\mathrm{surf}}}^2 R_{\mathrm{dis}} \quad (20)$$

where a parameter with the superscript "+" or "−" denotes the parameter related to the positive or negative solid particle, $P_{\mathrm{chg,inst}}$ and $P_{\mathrm{dis,inst}}$ are the instantaneous charge and discharge power capabilities, respectively, and λ is the product of γ and k.

It is well acknowledged that the cell aging and ambient temperature have a striking impact on battery power capability. The cell aging and temperature dependencies of the parameters in (19) and (20) should be considered for achieving more promising results in battery power capability prediction. In [32] and [33], the maximum possible concentration in the solid phase was expressed as being proportional to the capacity of the electrode. Thus, the permitted maximum surface concentration of the solid particle would also change with the cell aging level and can be formulated by

$$c_{\mathrm{surf,max}} = \alpha + \beta Q \quad (21)$$

where Q denotes the battery capacity, and α and β are two fitting coefficients for the maximum surface concentration.

Then, the maximum change of surface concentration can be rewritten as

$$\Delta c_{\mathrm{surf}} = \alpha + \beta Q - c_{\mathrm{surf},0}. \tag{22}$$

Combining (19), (20), and (22), the instantaneous available power capabilities at different cell aging levels can be calculated.

Moreover, the physiochemical properties of lithium-ion batteries are temperature dependent and obey the Arrhenius expression [34], [35]. The standard Arrhenius equation for computing a general physiochemical property value is defined as

$$\eta = \eta_{\mathrm{bas}} \exp\left[\frac{E_{\mathrm{act}}}{R}\left(\frac{1}{T} - \frac{1}{T_{\mathrm{bas}}}\right)\right] \tag{23}$$

where η denotes the physiochemical property value at ambient temperature T, η_{bas} the based physiochemical property value at the based temperature T_{bas} (namely 25 °C in the presented study), and E_{act} the activation energy.

As expressed in (19) and (20), the instantaneous available power capabilities of the battery are mainly governed by the lithium ion diffusion from electrolyte phase to solid phase, which is temperature dependent through the Arrhenius law, and consequently, the temperature dependent power capability can be determined by the Arrhenius expression. Equation (23) is a critical application in determining the rate of electrochemical reactions, while the activation energy is theoretically regarded as a constant. However, in most of practical cases, the activation energy changes with variation in temperature [36]. With this in consideration, the activation energy of battery power may be temperature dependent, and a modified Arrhenius equation for computing battery instantaneous available power is given by

$$P_{\mathrm{inst}} = P_{\mathrm{inst\_bas}} \exp\left[\frac{(\omega + \rho T)}{R}\left(\frac{1}{T} - \frac{1}{T_{\mathrm{bas}}}\right)\right] \tag{24}$$

where P_{inst} denotes the battery instantaneous available power ($P_{\mathrm{chg,inst}}$ for charge power and $P_{\mathrm{dis,inst}}$ for discharge power), $P_{\mathrm{inst\_bas}}$ the based instantaneous available power under the temperature of 25 °C, and ω and ρ are two fitting coefficients for the activation energy. It is noted that (19) and (20) are used for calculating the instantaneous charge and discharge power capabilities, respectively. The temperature dependence of the power capability is considered in (24). Based on the instantaneous charge and discharge power capabilities at the temperature of 25 °C computed by (19) and (20), the power capabilities at other temperatures can be obtained by (24).

IV. Verifications and Discussions

Since battery direct current resistance is typically employed for describing battery power capability, the battery charge and discharge power capabilities computed by using two recommended equations, i.e., (25), with direct current resistances in many studies and standards [37]–[39] are considered as the "real" values, i.e., the referenced power capabilities of the battery. In particular, the direct current resistance is determined by a current pulse and its resulting voltage change between 1 s after the start of the current pulse, which is consistent with the instantaneous time horizon for the power prediction:

$$\begin{cases} P_{\mathrm{ref,chg}} = V_{\max}(V_{\max} - V_{\mathrm{OCV}})/R_{\mathrm{chg}} \\ P_{\mathrm{ref,dis}} = V_{\min}(V_{\mathrm{OCV}} - V_{\min})/R_{\mathrm{dis}} \end{cases} \tag{25}$$

where $P_{\mathrm{ref,chg}}$ and $P_{\mathrm{ref,dis}}$ denote referenced charge and discharge power capabilities, respectively, and $V_{\max}$ and $V_{\min}$ the maximum terminal voltage and minimum terminal voltage, respectively. In this paper, $LiMn_2O_4$ batteries are used for the experiment and verification and, therefore, the maximum and minimum cell terminal voltages are set as 4.2 and 3.0 V, respectively. The referenced charge and discharge power capabilities at different cell aging levels and ambient temperatures are depicted in Figs. 4, 6, 7, and 9 in the following part and are used for parameter fitting.

A. Parameter Fitting

The Levenberg–Marquardt algorithm, also known as the damped least-squares method, has been widely applied to solve nonlinear least squares problems by finding a model curve so that the sum of the squares of the deviations between the experimental data and model computed values is minimized [40]–[42]. Due to its good performance in training model parameters, the Levenberg–Marquardt algorithm is employed to fit the parameters of (19), (20), (22), and (24) in a parameter optimization software called Auto2Fit. The optimal parameters for the positive and negative solid particles are listed in Table II.

Note that the coefficients of determination R^2 are 0.995 and 0.996 for instantaneous discharge and charge power capabilities, respectively. It means that the proposed models can well match the real relationships between the instantaneous available power capabilities and surface lithium concentrations of solid particles. The predictive results of instantaneous available power capabilities are elaborated in the following parts.

B. Instantaneous Charge Power Prediction

To investigate the effectiveness of the proposed approach during the process of battery aging, the battery cell with a rated capacity of 90 Ah degraded from 92 to 69.5 Ah was used for the verification. Fig. 4 shows the predictive results of battery instantaneous charge power at six various aging levels with the capacities of 92, 87, 82.5, 78.5, 74, and 69.5 Ah, respectively. It can be observed that the battery instantaneous available charge power decreases with the rising SOC, and the predictive power capabilities can track well with the referenced values for all the aging levels.

For evaluating the predictive accuracy of the proposed approach at different cell aging levels, one of the most common measures of forecast error, mean absolute percentage error (MAPE), is employed in the presented study and it is defined as

$$\mathrm{MAPE} = \frac{1}{n}\sum_{i=1}^{n} |(\mathrm{pre}_i - \mathrm{ref}_i)/\mathrm{ref}_i| \times 100\% \tag{26}$$

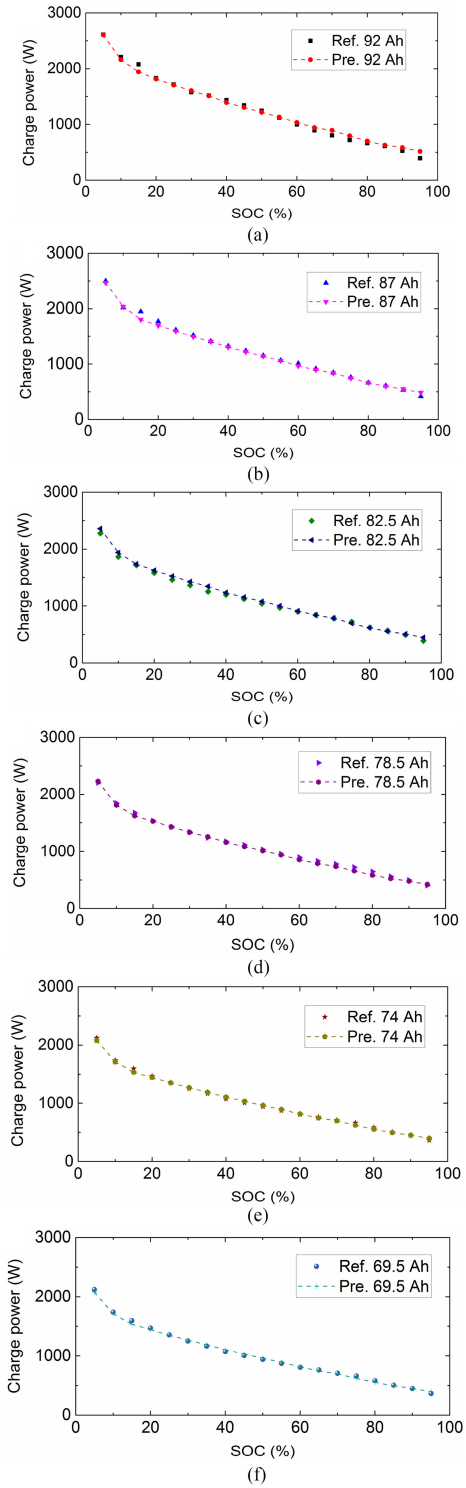

Fig. 4. Battery instantaneous charge power prediction results at different aging levels, where (a) 92 Ah, (b) 87 Ah, (c) 82.5 Ah, (d) 78.5 Ah, (e) 74 Ah, and (f) 69.5 Ah.

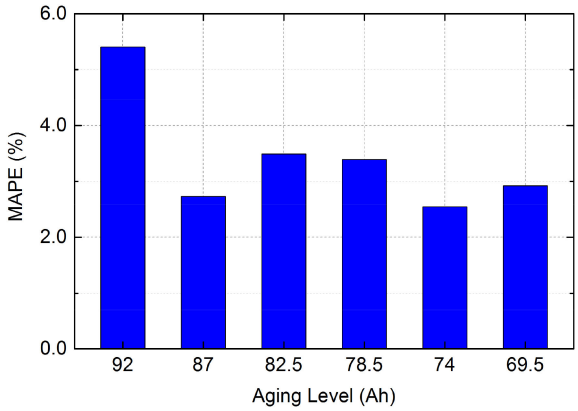

Fig. 5. MAPEs of battery instantaneous charge power prediction at different aging levels.

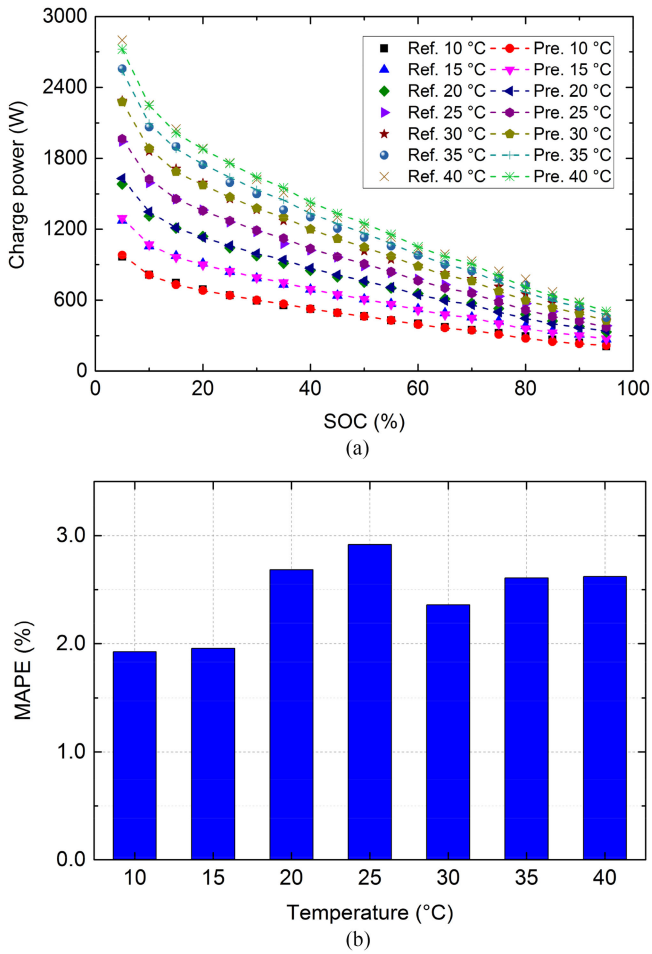

Fig. 6. Battery instantaneous charge power prediction results at various temperatures, where (a) referenced and predictive power capabilities and (b) MAPEs.

where pre_i and ref_i denote the predictive and referenced values, respectively, and n denotes the number of data set of predictive and referenced values.

The MAPEs of battery instantaneous charge power prediction at different aging levels are depicted in Fig. 5, where the maximum MAPE is about 5.4% at the capacity of 92 Ah. This relatively large error is attributed to the influence of few outliers in the prediction. However, promising results with the MAPEs of less than 3.5% can be obtained at other aging levels. It indicates that the proposed method can well handle different cell aging levels.

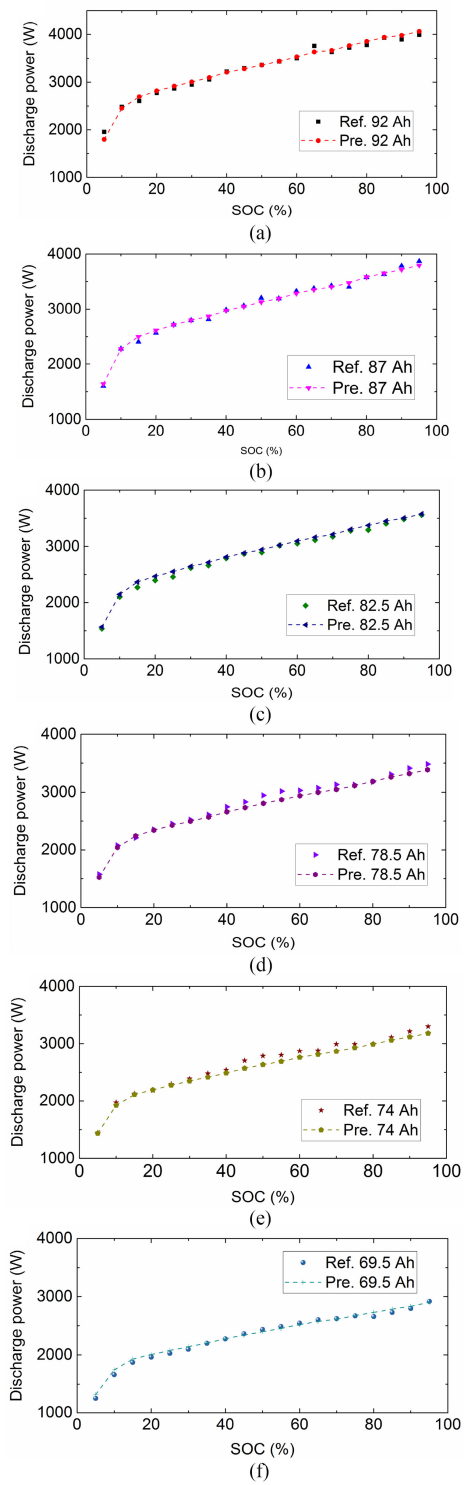

Fig. 7. Battery instantaneous discharge power prediction results at different aging levels, where (a) 92 Ah, (b) 87 Ah, (c) 82.5 Ah, (d) 78.5 Ah, (e) 74 Ah, and (f) 69.5 Ah.

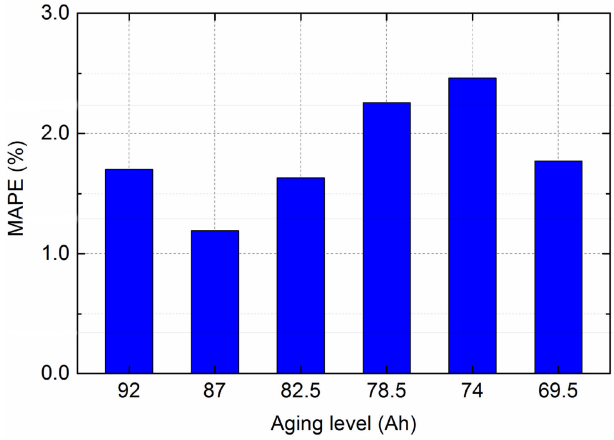

Fig. 8. MAPEs of battery instantaneous discharge power prediction at different aging levels.

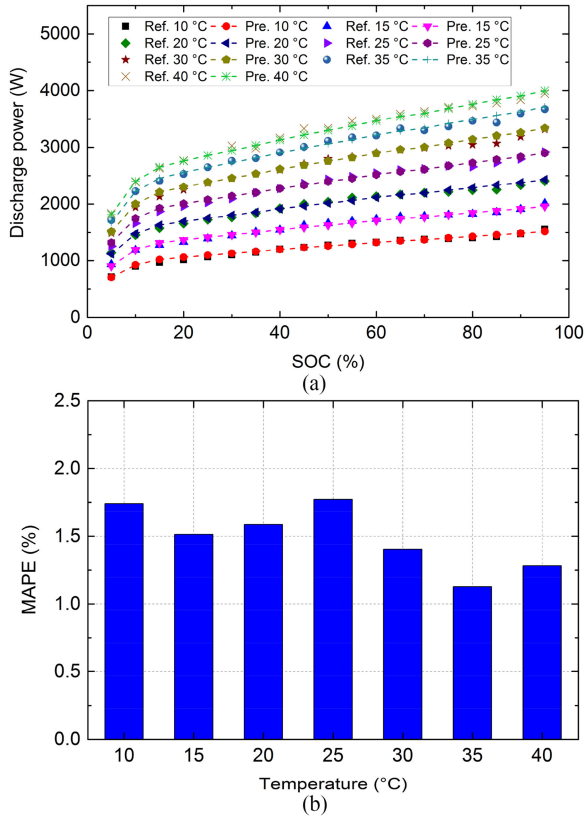

Fig. 9. Battery instantaneous discharge power prediction results at various temperatures, where (a) referenced and predictive power capabilities and (b) MAPEs.

To assess the adaptability of the proposed method at various temperatures, the battery was loaded at a commonly used temperature ranging from 10 to 40 °C with the interval of 5 °C for the verification. Fig. 6(a) compares battery instantaneous charge power prediction results with referenced data at various SOCs and ambient temperatures, showing that the forecasts are able to follow the tracks of the referenced values. It can also be seen that the ambient temperature has a significant impact on the power capabilities, which decrease with the declining temperature at some battery SOCs. Furthermore, the MAPEs of the prediction results are presented in Fig. 6(b), where all the MAPEs are limited in a small error band of 3.0%, indicating the proposed method can work well and achieve desirable results at various ambient temperatures.

TABLE II
OPTIMAL PARAMETERS FOR THE POSITIVE AND NEGATIVE SOLID PARTICLES

Parameter	Positive solid particle coefficient	Negative solid particle coefficient
σ	1.854×10^{-7}	1.356×10^{-7}
λ	1.075×10^{-16}	1.034×10^{-15}
ε	2.000×10^{-3}	1.631×10^{-3}
α	7.958×10^{2}	2.995×10^{2}
β	1.496×10^{3}	3.585×10^{3}
ω	54.670	63.184
ρ	-1.911×10^{4}	-2.180×10^{4}
R^2	0.995	0.996

C. Instantaneous Discharge Power Prediction

Likewise, the battery operated at six different aging levels are used for evaluating the instantaneous discharge power prediction, and the predictive results are demonstrated in Fig. 7. It is clear that the battery instantaneous discharge power increases with the rising SOC, which shows an opposite tendency in comparison with the instantaneous charge power, and the predictive power capabilities can effectively follow this trend and approach the referenced values at different aging levels.

Fig. 8 provides the MAPEs of battery instantaneous discharge power prediction results. It can be observed that at various aging levels, the MAPEs are within 2.50%, which highlights the robustness of the proposed method in forecasting battery instantaneous discharge power against varying battery aging.

Additionally, the referenced and predictive results of battery instantaneous discharge power at different ambient temperatures are compared in Fig. 9(a), and their MAPEs are depicted in Fig. 9(b). From Fig. 9(a), it can be seen that as the ambient temperature rises, the magnitude of the discharge power capability increases at some battery SOCs. Moreover, the instantaneous discharge power forecasts can still tail after the referenced data. It is noteworthy that the MAPEs showed in Fig. 9(b) are successfully confined into a narrow error band of 2.0%, which validates the feasibility of the proposed method for the instantaneous discharge power prediction.

According to the close agreement between the forecasts and experimental data, it can be summarized that the proposed method for both battery instantaneous available charge and discharge power capabilities prediction can handle various cell aging levels and ambient temperatures quite well.

V. CONCLUSION

This paper proposes a physical mechanism-based power prediction method for lithium-ion batteries. Based on the theoretical analysis of battery Gibbs power and dissipation power of its internal resistance, quantitative relationships between battery surface lithium concentration and instantaneous charge and discharge power capabilities are deduced and applied for the power capability prediction. Different from conventional methods for battery power capability prediction with macroscopically observed variables such as the cell terminal voltage and current as the constrained limits, a physical limit, i.e., the lithium concentration limit of the solid particle is employed in the proposed relation, providing a direct insight into electrochemical processes inside batteries. The factors that would influence battery power capabilities, such as cell aging and ambient temperature, are considered in the proposed relations, and their parameters are figured out using the Levenberg–Marquardt algorithm. The proposed method is verified with various cell aging levels and ambient temperatures, and the experimental results demonstrate the close agreement between the forecasts and referenced values. Most of the MAPEs of the forecasts at various battery operation conditions are less than 3.5%, which highlights the superior accuracy and robustness of the proposed method.

Since the lithium concentration is obtained by operating an EM, the implementation task of the proposed method can be really tough for microprocessor units, especially in low-cost target BMSs. It is recommended to further simplify the EM for reducing the complexity of the algorithm. The microprocessors with 32/64 bits or dual/multicores and cloud-based BMSs are promising to implement battery EM and the proposed algorithm. Note that the proposed method only used the surface lithium concentration for the power prediction within a short-term time horizon, i.e., 1 s, in this paper. Since the prediction within a longer time horizon such as 10 s and 30 s is also meaningful in applications, the long-term prediction needs to be investigated. For the long-term prediction, not only the change of surface lithium concentration but also the changes of lithium concentrations at various radii of the solid particle should be considered in the algorithm. These tasks will be further investigated in our next stage.

ACKNOWLEDGMENT

The authors would like to thank the National Active Distribution Network Technology Research Center, Beijing Jiaotong University, for the prior work on battery tests.

REFERENCES

[1] J. Cho, S. Jeong, and Y. Kim, "Commercial and research battery technologies for electrical energy storage applications," *Prog. Energy Combustion Sci.*, vol. 48, pp. 84–101, 2015.
[2] M. Cacciato, G. Nobile, G. Scarcella, and G. Scelba, "Real-time model-based estimation of SOC and SOH for energy storage systems," *IEEE Trans. Power Electron.*, vol. 32, no. 1, pp. 794–803, Jan. 2017.
[3] Z. Wang, J. Ma, and L. Zhang, "Finite element thermal model and simulation for a cylindrical Li-ion battery," *IEEE Access*, vol. 5, pp. 15372–15379, 2017.
[4] J. Kim, J. Shin, C. Chun, and B. H. Cho, "Stable configuration of a Li-ion series battery pack based on a screening process for improved voltage/SOC balancing," *IEEE Trans. Power Electron.*, vol. 27, no. 1, pp. 411–424, Jan. 2012.
[5] Z. Zhang, X. Cheng, Z. Lu, and D. Gu, "SOC estimation of lithium-ion batteries with AEKF and wavelet transform matrix," *IEEE Trans. Power Electron.*, vol. 32, no. 10, pp. 7626–7634, Oct. 2017.
[6] Z. Wei, C. Zou, F. Leng, B. H. Soong, and K. J. Tseng, "Online model identification and state of charge estimate for Lithium-ion battery with a recursive total least squares-based observer," *IEEE Trans. Ind. Electron.*, vol. 65, no. 2, pp. 1336–1346, Feb. 2018.
[7] L. Zheng, J. Zhu, G. Wang, T. He, and Y. Wei, "Novel methods for estimating Lithium-ion battery state of energy and maximum available energy," *Appl. Energy*, vol. 178, pp. 1–8, 2016.
[8] Z. Zhang, X. Cheng, Z. Lu, and D. Gu, "SOC estimation of Lithium-ion battery pack considering balancing current," *IEEE Trans. Power Electron.*, vol. 33, no. 3, pp. 2216–2226, Mar. 2018.

[9] A. Farmann and D. U. Sauer, "A comprehensive review of on-board state-of-available-power prediction techniques for Lithium-ion batteries in electric vehicles," *J. Power Sources*, vol. 329, pp. 123–137, 2016.
[10] C. Chen, R. Xiong, and W. Shen, "A Lithium-ion battery-in-the-loop approach to test and validate multi-scale dual H infinity filters for state of charge and capacity estimation," *IEEE Trans. Power Electron.*, vol. 33, no. 1, pp. 332–342, Jan. 2018.
[11] X. Hu, C. Zou, C. Zhang, and Y. Li, "Technological developments in batteries: A survey of principal roles, types, and management needs," *IEEE Power Energy Mag.*, vol. 15, no. 5, pp. 21–31, Sep./Oct. 2017.
[12] C. Burgos-Mellado, M. E. Orchard, M. Kazerani, R. Cárdenas, and D. Sáez, "Particle-filtering-based estimation of maximum available power state in lithium-ion batteries," *Appl. Energy*, vol. 161, pp. 349–363, 2016.
[13] F. Zheng, J Jiang, B. Sun, W. Zhang, and M. Pecht, "Temperature dependent power capability estimation of Lithium-ion batteries for hybrid electric vehicles," *Energy*, vol. 113, pp. 64–75, 2016.
[14] C. Fleischer, W. Waag, Z. Bai, and D. U. Sauer, "Adaptive on-line state-of-available-power prediction of Lithium-ion batteries," *J. Power Electron.*, vol. 13, no. 4, pp. 516–527, 2013.
[15] W. Haiying, H. Zhonghua, H. Yu, and L. Gechen, "Power state prediction of battery based on BP neural network," in *Proc. Int. Forum Strategic Techol.*, 2012, pp. 1–4.
[16] A. A. Hussein, "A neural network based method for instantaneous power estimation in electric vehicles' Li-ion batteries," in *Proc. IEEE Appl. Power Electron. Conf. Expo.*, 2017, pp. 3122–3126.
[17] F. Sun, R. Xiong, H. He, W. Li, and J. E. E. Aussems, "Model-based dynamic multi-parameter method for peak power estimation of Lithium–ion batteries," *Appl. Energy*, vol. 96, pp. 378–386, 2012.
[18] W. Zhang, W. Shi, and Z. Ma, "Adaptive unscented Kalman filter based state of energy and power capability estimation approach for Lithium-ion battery," *J. Power Sources*, vol. 289, pp. 50–62, 2015.
[19] X. Hu, R. Xiong, and B. Egardt, "Model-based dynamic power assessment of Lithium-ion batteries considering different operating conditions," *IEEE Trans. Ind. Informat.*, vol. 10, no. 3, pp. 1948–1959, Aug. 2014.
[20] Z. Wei, S. Meng, K. J. Tseng, T. M. Lim, B. H. Soong, and M. Skyllas-Kazacos, "An adaptive model for vanadium redox flow battery and its application for online peak power estimation," *J. Power Sources*, vol. 344, pp. 195–207, 2017.
[21] J. Jiang, S. Liu, Z. Ma, L. Y. Wang, and K. Wu, "Butler-volmer equation-based model and its implementation on state of power prediction of high-power lithium titanate batteries considering temperature effects," *Energy*, vol. 117, pp. 58–72, 2016.
[22] L. Zheng, L. Zhang, J. Zhu, G. Wang, and J. Jiang, "Co-estimation of state-of-charge, capacity and resistance for Lithium-ion batteries based on a high-fidelity electrochemical model," *Appl. Energy*, vol. 180, pp. 424–434, 2016.
[23] K. Smith and C. Wang, "Pulse discharge power availability of a Lithium-ion hybrid vehicle battery pack," SAE Tech. Paper, 2005-01-3464, 2005. [Online]. Available: https://doi.org/10.4271/2005-01-3464
[24] Y. S. Meng and M. E. Arroyo-de Dompablo, "First principles computational materials design for energy storage materials in lithium ion batteries," *Energy Environ. Sci.*, vol. 2, no. 6, pp. 589–609, 2009.
[25] N. A. Chaturvedi, R. Klein, J. Christensen, J. Ahmed, and A. Kojic, "Algorithms for advanced battery-management systems," *IEEE Control Syst.*, vol. 30, no. 3, pp. 49–68, Jun. 2010.
[26] W. van Egmond, U. K Starke, M. Saakes, C. J. N. Buisman, and H. V. M. Hamelers, "Energy efficiency of a concentration gradient flow battery at elevated temperatures," *J. Power Sources*, vol. 340, pp. 71–79, 2017.
[27] C. Zou, C. Manzie, D. Nešić, and A. G. Kallapur, "Multi-time-scale observer design for state-of-charge and state-of-health of a Lithium-ion battery," *J. Power Sources*, vol. 335, pp. 121–130, 2016.
[28] S. J. Moura, N. A. Chaturvedi, and M. Krstic, "PDE estimation techniques for advanced battery management systems—Part I: SOC estimation," in *Proc. Amer. Control Conf.*, 2012, pp. 559–565.
[29] X. Han, M. Ouyang, L. Lu, and J. Li, "Simplification of physics-based electrochemical model for lithium ion battery on electric vehicle. Part I: Diffusion simplification and single particle model," *J. Power Sources*, vol. 278, pp. 802–813, 2015.
[30] X. Hu, D. Cao, and B. Egardt, "Condition monitoring in advanced battery management systems: Moving horizon estimation using a reduced electrochemical model," *IEEE/ASME Trans. Mechatronics*, doi: 10.1109/TMECH.2017.2675920.
[31] W. Waag, S. Käbitz, and D. U. Sauer, "Experimental investigation of the lithium-ion battery impedance characteristic at various conditions and aging states and its influence on the application," *Appl. Energy*, vol. 102, pp. 885–897, 2013.
[32] R. Klein *et al.*, "Electrochemical model based observer design for a lithium-ion battery," *IEEE Trans. Control Syst. Technol.*, vol. 21, no. 2, pp. 289–301, Mar. 2013.
[33] K. Smith and C. Wang, "Solid-state diffusion limitations on pulse operation of a Lithium ion cell for hybrid electric vehicles," *J. Power Sources*, vol. 161, no. 1, pp. 628–639, 2006.
[34] K. Smith and C. Wang, "Power and thermal characterization of a Lithium-ion battery pack for hybrid-electric vehicles," *J. Power Sources*, vol. 160, no. 1, pp. 662–673, 2006.
[35] F. Zheng, J. Jiang, B. Sun, W. Zhang, and M. Pecht, "Temperature dependent power capability estimation of Lithium-ion batteries for hybrid electric vehicles," *Energy*, vol. 113, pp. 64–75, 2016.
[36] M. Ikeda and M. Aniya, "Bond strength—Coordination number fluctuation model of viscosity: An alternative model for the vogel-fulcher-tammann equation and an application to bulk metallic glass forming liquids," *Materials*, vol. 3, no. 12, pp. 5246–5262, 2010.
[37] J. R. Belt, "Battery test manual for plug-in hybrid electric vehicles," Idaho Nat. Lab., Idaho Falls, ID, USA, Tech. Rep. INL/EXT-07-12536, Dec. 2010.
[38] C. Zhang, C. Zhang, and S. Sharkh, "Estimation of real-time peak power capability of a traction battery pack used in an HEV," in *Proc. Asia-Pac. Power Energy Eng. Conf.*, 2010, pp. 1–6.
[39] G. L. Plett, "High-performance battery-pack power estimation using a dynamic cell model," *IEEE Trans. Veh. Technol.*, vol. 53, no. 5, pp. 1586–1593, Sep. 2004.
[40] K. Levenberg, "A method for the solution of certain non-linear problems in least squares," *Quart. Appl. Math.*, vol. 2, no. 2, pp. 164–168, 1944.
[41] D. W. Marquardt, "An algorithm for least-squares estimation of nonlinear parameters," *J. Soc. Ind. Appl. Math.*, vol. 11, no. 2, pp. 431–441, 1963.
[42] J. J. Moré, "The levenberg-marquardt algorithm: Implementation and theory," in *Numerical Analysis Anonymous*. New York, NY, USA: Springer, 1978, pp. 105–116.

Linfeng Zheng (S'14) received the B.E. and M.E. degrees in electrical engineering from Beijing Jiaotong University, Beijing, China, in 2011 and 2014, respectively. He is currently working toward the Ph.D. degree in electrical engineering at the University of Technology Sydney, Ultimo, NSW, Australia.

His research interest includes the development of battery and supercapacitor management and packaging techniques for electric vehicles and energy storage systems.

Jianguo Zhu (S'93–M'96–SM'03) received the B.E. degree from the Jiangsu Institute of Technology, Zhenjiang, China, in 1982, the M.E. degree from the Shanghai University of Technology, Shanghai, China, in 1987, and the Ph.D. degree from the University of Technology Sydney (UTS), Ultimo, NSW, Australia, in 1995, all in electrical engineering.

He is currently a Professor with School of Electrical and Data Engineering, UTS. His current research interests include electromagnetics, magnetic properties of materials, electrical machines and drives, power electronics, and green energy systems.

Guoxiu Wang received the Ph.D. degree in materials engineering from the University of Wollongong, Wollongong, NSW, Australia, in 2001.

He is currently a Distinguished Professor with the School of Mathematical and Physical Sciences, University of Technology Sydney, Ultimo, NSW, Australia, and the Director of the Centre for Clean Energy Technology, University of Technology Sydney. His research interests include electromaterials for applications in rechargeable Lithium-ion battery, lithium-air batteries, sodium-ion batteries, lithium–sulfur batteries, supercapacitors, and fuel-cells, controllable synthesis of one-dimensional semiconductor nanostructures and their applications for chemical and biosensors, and semiconductor quantum dots, and quantum wires and quantum tubes for nanoscale electronic and photonic devices.

Dylan Dah-Chuan Lu (M'04–SM'09) received the B.E. and Ph.D. degrees in electrical engineering from The Hong Kong Polytechnic University, Hong Kong, in 1999 and 2004, respectively.

In 2003, he joined the PowereLab Ltd., as a Senior Design Engineer and was responsible for industrial switching power supply projects. He was a full-time faculty member with The University of Sydney from 2006 to 2016. He now holds an honorary position at the University of Sydney. Since July 2016, he has been an Associate Professor with the School of Electrical and Data Engineering, University of Technology Sydney, Ultimo, NSW, Australia. His current research interest includes efficient and reliable power conversion for renewable sources, energy storage systems, and microgrids.

Dr. Lu was the recipient of the Best Paper Award in the category of Emerging Power Electronic Technique at the IEEE PEDS 2015. He is currently an Associate Editor for the IEEE TRANSACTIONS ON CIRCUITS AND SYSTEMS II and the *IET Renewable Power Generation*. He is a member of the Engineers Australia.

Tingting He (S'14) received the B.S. and Master's degrees from Beijing Jiaotong University, Beijing, China, in 2009 and 2015, respectively, both in electrical engineering. She is currently working toward the Ph.D. degree in electrical engineering at the School of Electrical and Data Engineering, University of Technology Sydney, Ultimo, NSW, Australia.

Her research interests include power electronics, electric vehicles, and predictive control.